

Supporting information (SI)

**Chromophore-Removal-Induced Conformational Change in Photoactive Yellow Protein
Determined through Spectroscopic and X-ray Solution Scattering Studies**

Youngmin Kim^{†‡§}, Prabhakar Ganesan^{†§}, Junbeom Jo^{†‡}, Seong Ok Kim^{†‡}, Kamatchi
Thamilselvan^{†‡}, and Hyotcherl Ihee^{†‡*}

[†]Department of Chemistry and KI for the BioCentury, Korea Advanced Institute of Science and
Technology (KAIST), Daejeon 305-701, Republic of Korea

[‡]Center for Nanomaterials and Chemical Reactions, Institute for Basic Science (IBS), Daejeon
305-701, Republic of Korea

[§]These authors contributed equally.

* Corresponding author: E-mail: *hyotcherl.ihee@kaist.ac.kr*

Supporting Method

Protein Purification and Sample Preparation. The reconstructed apo-PYP in the pQE30 vector was over-expressed in *E. coli* BL21 (DE3) by IPTG induction, reconstituted with *p*-coumaric anhydride, and purified through Ni affinity chromatography and ion-exchange chromatography, as described previously.¹⁻² The purified protein was further diluted in 20 mM Tris buffer (pH 7.0, 20 mM NaCl) or 400 mM Tris buffer (pH 7.0), depending on the experimental requirements. Samples were prepared in the following order: PYP without hydroxylamine, and PYP with hydroxylamine. Two groups of samples were used for the UV/VIS spectroscopic and SAXS measurements. For the bleached sample, we mixed the PYP with hydroxylamine 1 day before the measurement. The conditions were 400 mM Tris buffer (pH 7.0) and 300 mM hydroxylamine, with a 10 mg/mL protein concentration. The samples were dialyzed with 20 mM Tris (pH 7.0) and 20 mM NaCl.

Matrix-Assisted Laser Desorption/Ionization Time-Of-Flight (MALDI-TOF). Molecular weights of PYP and bleached PYP (PYP with the chromophore removed) were measured using a MALDI-TOF mass spectrometer (Bruker Autoflex III, Bruker Daltonics Inc., Germany). Sinapinic acid was used as a matrix material for the measurement. The laser source for MALDI-TOF was the third harmonic of a Nd:YAG laser (355 nm), and the repetition rate was 1 Hz.

Circular Dichroism. To confirm the secondary structure of the PYP and bleached PYP, circular dichroism (CD) spectrum was measured using a CD spectrometer (Jasco-815, JASCO Inc., Japan) with a 1-mm quartz cuvette at room temperature. The spectral window ranged from 190

nm to 260 nm at 1-nm intervals. The baseline was measured with the same buffer in the same cuvette and subtracted.

Time-Resolved UV/VIS Spectroscopy. The PYP chromophore cutting progress was measured using UV/VIS spectroscopy (UV-2550, Shimadzu). The sample was diluted to the desired concentration for the bleaching experiment (300–500 mM hydroxylamine for 14 μ M photoactive yellow protein). UV/VIS absorption spectra of the incubated reaction were recorded continuously until complete bleaching of PYP occurred. The time-resolved UV/VIS spectra thus recorded were subsequently used for decay analysis. Separate bleaching reactions were performed to determine the relationship between the concentration of the hydroxylamine (300, 350, and 400 mM) and the bleaching decay constant. Increasing the concentration of hydroxylamine beyond 450 mM caused the protein to precipitate. When the concentration of hydroxylamine was excessively high, compared to that of PYP, the decay time is proportional to the concentration of PYP with pseudo-first order and the rate constant can be expressed as follows;

$$r = k'[PYP] \quad \text{where } k' = k[H_0] \text{ and } [H_0] = \text{initial hydroxylamine concentration}$$

Experiment-Restrained Rigid-Body MD Simulation. This method was almost identical to that in a previous study.³ In experiment-restrained rigid-body MD simulation, a crystal structure (2PHY) was used as a starting point. The structures were divided into a number of rigid bodies comprising several amino acids. The rigid bodies were allowed to move under the influence of the chemical and χ^2 force field. Because the atomic structure within a rigid body is constrained to

be the same as that of the crystal or NMR structure, the force field within the rigid body is not considered; however, the Van der Waals interactions between rigid bodies and the N-C bond-length corrections between rigid bodies are included in the chemical force field. The χ^2 force field is introduced to drive the molecular structure generated by MD simulations toward a structure that yields a difference scattering curve that matches the experimental difference scattering curve. Thus, the total potential (U) on the rigid bodies has the Van der Waals term (U_{LJ}), the χ^2 term, and the bond correction term (B_{ij}) as follows:

$$U = c_1 U_{LJ} + c_2 \chi^2 + c_3 B_{ij} \quad (1)$$

where c_1 , c_2 and c_3 are the weighting parameters to scale the magnitude of the three terms appropriately. U_{LJ} and χ^2 , which define the agreement between the experimental data and theoretical value, are as follows; the scaling factor c_s and reduced units are used.

$$U_{LJ} = \sum_{i=1}^N \sum_{j \neq i}^N 4 \left(\frac{\sigma^{12}}{r_{ij}^{12}} - \frac{\sigma^6}{r_{ij}^6} \right) \quad (2)$$

$$\chi^2 = \sum_{q=1}^{N_q} \left(\frac{I_{\text{exp}}(q) - c_s I_{\text{cal}}(q)}{\sigma_q} \right)^2 \quad (3)$$

The force field is the gradient of the total potential; therefore, the total force acting on the i -th particle among total number of particles, N is as follows:

$$\begin{aligned} \mathbf{f}_i &= -\nabla_i U \\ &= 24c_1 \sum_{j \neq i}^N \left(2 \frac{\sigma^{12}}{r_{ij}^{13}} - \frac{\sigma^6}{r_{ij}^7} \right) \\ &\quad + 2c_2 c_s \sum_{q=1}^{N_q} \left(\frac{I_{\text{exp}}(q) - c_s I_{\text{cal}}(q)}{\sigma_q^2} \right) \sum_{j \neq i}^N f_i^s(q) f_j^s(q) \left(\cos(qr_{ij}) - \frac{\sin(qr_{ij})}{qr_{ij}} \right) \frac{\mathbf{r}_{ij}}{r_{ij}^2} \end{aligned} \quad (4)$$

In the L-J potential, σ is defined as the r value where the corresponding potential is zero and \mathbf{r}_{ij} ($= \mathbf{r}_i - \mathbf{r}_j$) is the distance between particle i and particle j . If the distance between the two particles is smaller than σ , the repulsion increases steeply. We defined the following two types of σ values for the L-J potential between rigid bodies. For the N-C bond between two rigid bodies consisting of helices, $\sigma_{\text{N-C}} = 1.28 \text{ \AA}$, and for the atoms between two rigid bodies, $\sigma_{\text{a-a}} = 1.2 \text{ \AA}$. In the bond correction term, B_{ij} simply maintains the distance between rigid bodies at the initial value. Once the total forces between rigid bodies were determined, MD simulations were run on the basis of Newtonian equations. The coordinate of the center of mass (COM) of the rigid body was as follows:

$$\mathbf{R} = \frac{\sum m_i \mathbf{r}_i}{M}, \quad (5)$$

where m_i and \mathbf{r}_i are the mass and position of the i -th atom of the rigid-body and M is the mass of a rigid body ($M = \sum_i m_i$).

The COM moved translationally, and the relative rotational motion with respect to the COM determined the relative position ($\mathbf{r}'_i = \mathbf{r}_i - \mathbf{R}$) of the i -th atom referenced to \mathbf{R} , \mathbf{r}'_i . At each step of the MD simulation, \mathbf{R} , \mathbf{r}_i and \mathbf{r}'_i were updated. The equation for the translational motion of the COM is as follows:

$$\ddot{\mathbf{R}} = \frac{\mathbf{F}}{M}. \quad (6)$$

where $\mathbf{F} = \sum_i \mathbf{f}_i$ is the total force on the rigid body as the sum of \mathbf{f}_i acting on the i -th atom

within the rigid body. The total torque acting on each rigid body with respect to the COM is as follows:

$$\mathbf{N} = \sum_i \mathbf{r}_i' \times \mathbf{f}_i. \quad (7)$$

The velocity of \mathbf{r}_i' relative to \mathbf{R} is as follows:

$$\dot{\mathbf{r}}_i' = \boldsymbol{\omega} \times \mathbf{r}_i' \quad (8)$$

where $\boldsymbol{\omega}$ is the angular velocity with respect to the COM of the rigid body. The moment of inertia with respect to the COM is as follows:

$$\mathbf{I} = \begin{bmatrix} \sum m_i (y_i'^2 + z_i'^2) & -\sum m_i x_i' y_i' & -\sum m_i x_i' z_i' \\ -\sum m_i x_i' y_i' & \sum m_i (x_i'^2 + z_i'^2) & -\sum m_i y_i' z_i' \\ -\sum m_i x_i' z_i' & -\sum m_i y_i' z_i' & \sum m_i (x_i'^2 + y_i'^2) \end{bmatrix} \quad (9)$$

The rotational equation of motion of a rigid body around \mathbf{R} can be expressed as⁴:

$$\dot{\boldsymbol{\omega}} = \mathbf{I}^{-1} \cdot (\mathbf{N} - \boldsymbol{\omega} \times (\mathbf{I} \cdot \boldsymbol{\omega})) \quad (10)$$

Eq. (5) updates \mathbf{R} and combining eqns. (7)–(10) updates \mathbf{r}_i' .

Molecular Dynamics Simulation. MD simulation of PYP with cleavage of the bond between the chromophore and protein core provides an insight into the mechanism underlying chromophore migration from the hydrophobic core into the solution. All MD simulations were performed using GROMACS⁵ with the AMBER03⁶ force field. The crystal structure of ground-state PYP (holo-PYP, PDB code: 1NWZ) solved at a resolution of 0.85 Å. was downloaded from the

Protein Data Bank⁷ and used as initial coordinates. Force field parameters of the ground state chromophore were kindly provided by Professor Gerrit Groenhof. We performed the molecular dynamics simulation of chromophore migration subsequent to chemical detachment from the PYP Cys69 residue. The detachment of the chromophore from the Cys69 residue was performed using an “instantaneous” model. The bond between the sulfur of Cys69 in PYP and carbon of the chromophore was severed to simulate instantaneous detachment. Molecular dynamics simulation of PYP with unbound chromophore in the active site pocket was performed to examine chromophore migration outside the protein. The protein along with the chromophore in the binding pocket was embedded in a cubic water box and simulated with periodic boundary conditions. A single point charge (SPC) model was used for water molecules. The distance between the proteins and the edge of the water box was maintained at 10 Å. After the initial constrained minimization with the steepest descent, the system was heated to 300 K in step-wise mode by performing a NVT (constant number of atoms N, volume V, and temperature T) simulation for approximately 100 ps for relaxation of solvent molecules. The system was then equilibrated for 100 ps at 1 atmospheric pressure preceding the production run with a time step of 2 fs. Thereafter, the generated coordinates were used for obtaining the structural aspects of the path for the chromophore to move from the protein interior binding pocket to the solvent exterior. However, accurate conformational change cannot directly be inferred from this MD analysis results because of differences in terms of the solvent/buffer in the molecular dynamics simulation. Nonetheless, MD simulation of the photo-detached PYP with an unbound chromophore revealed the migration path of the chromophore from the active site pocket to the solvent in the exterior of the protein. The migration of the chromophore from the interior of the

protein to the exterior solvent occurred within 100 ps of MD simulation time. Details related to the amino acid residues that interact with the chromophore during migration are presented in Table S2. The results show that the chromophore directly exits from the inner pocket of the protein to the solvent. Therefore, there is no intermediate state.

Potential Energy Calculations of Holo-PYP, PYP Without Chromophore, and pB₂ in Solution.

Potential energies of the protein molecules were calculated using GROMACS⁵ with the AMBER03⁶ force field. The PYP pG (1NWZ) crystals structure, which are obtained at pH 7 and have a space group P63, and pB₂ solution structure (2KX6) were retrieved from the Protein Data Bank⁷. The coordinates of the protein without crystal water molecules were energy-minimized using a convergent energy-minimization method in vacuum to determine the potential energy of the native structure. In each case, the minimization protocol included 10,000 steps of the steepest descent algorithm until convergence to machine precision. The convergence of the energy minimization was achieved when the maximum force was less than 10 kJ mol⁻¹ nm⁻¹ or until no substantial improvement could be attained between steps. A short-range cutoff distance of 6 Å was used for van-der-Waals and Coulomb interactions and a 9 Å cutoff distance was utilized for the long-range neighbor list to consider the long-range interactions. In all three cases, namely pG with chromophore (1NWZ), pG without the chromophore (the chromophore was removed in pG), and pB₂ (2KX6), the convergence of energy minimization occurred between 5,000 and 6,000 steps of the steepest descent minimization.



Figure S1. Flow cell system for SAXS measurement at Pohang Light Source. The sample is continuously injected using the syringe pump. The X-ray scattering pattern was measured using a quartz capillary in the flow cell available in the beamline.

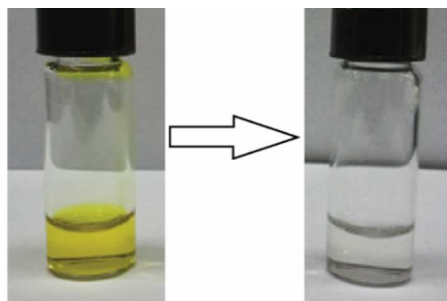


Figure S2. Bleaching of photoactive yellow protein by hydroxylamine without any precipitation.

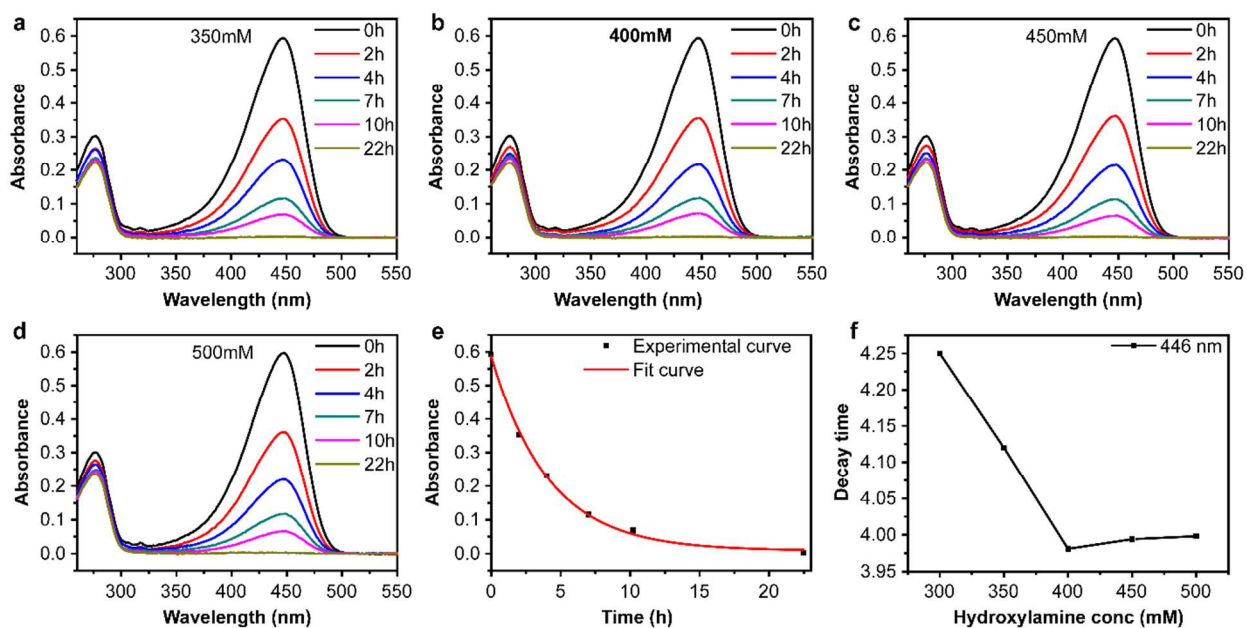


Figure. S3. Effect of hydroxylamine concentration from 350 mM to 500 mM on photoactive yellow protein (14 μM) bleaching as determined by UV/VIS spectrum and decay constants.

(a-d) shows time-resolved UV-VIS spectra for effect of hydroxylamine at concentrations from

350 mM to 500 mM. (e) Figure shows fitting curve at 350 mM using one exponential decay. (f) Plot of the decay time point at each hydroxylamine concentration. ($k = \sim 1.94 \text{ M}^{-1} \cdot \text{h}^{-1}$).

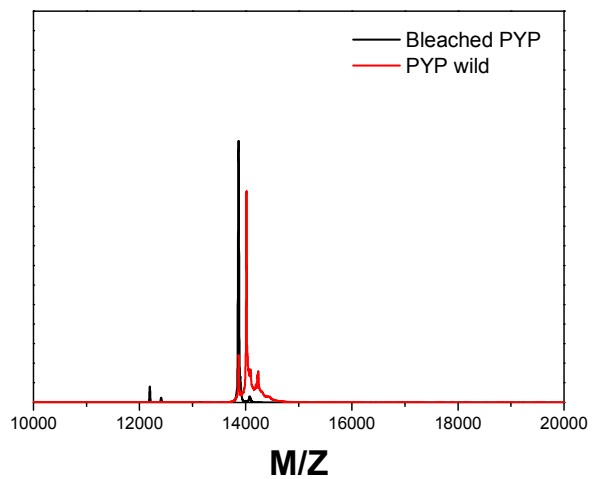


Figure S4. MALDI/TOF results for holo-PYP (red, 14.0 k) and bleached PYP (black, 13.90 k).

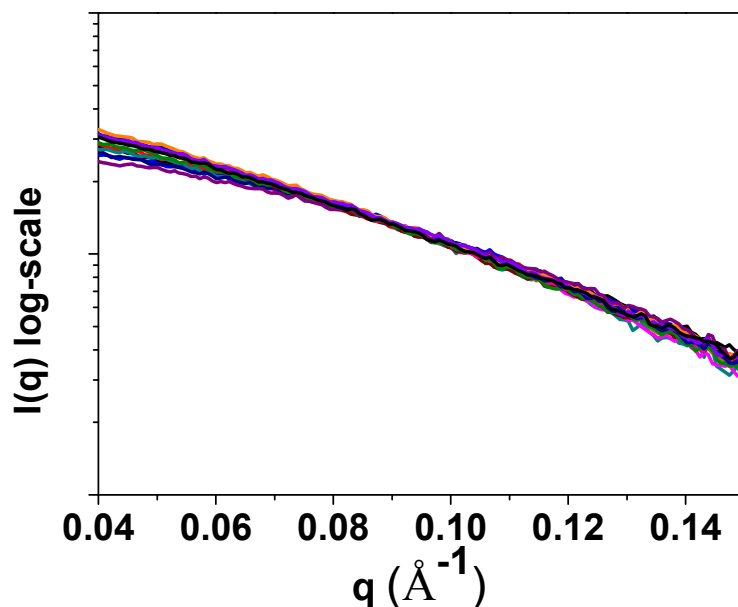


Figure S5. X-ray solution scattering data of PYP bleaching in the SAXS region at various time points (0 h to 15 h). For the bleaching reaction for the SAXS experiment, incubation was performed for 15 h with a PYP concentration of 10 mg/mL in 350 mM Tris, pH 7.0, and 400 mM hydroxylamine. Time-resolved SAXS measurement with a 1-h interval showed that PYP with the chromophore removed had a different shape, indicating that the structure was changed by chromophore removal. The curves intersect at $q = 0.095 \text{ \AA}^{-1}$; therefore, we used $q = 0.095 \text{ \AA}^{-1}$ as the normalization point for scaling PYP and bleached PYP SAXS curves.

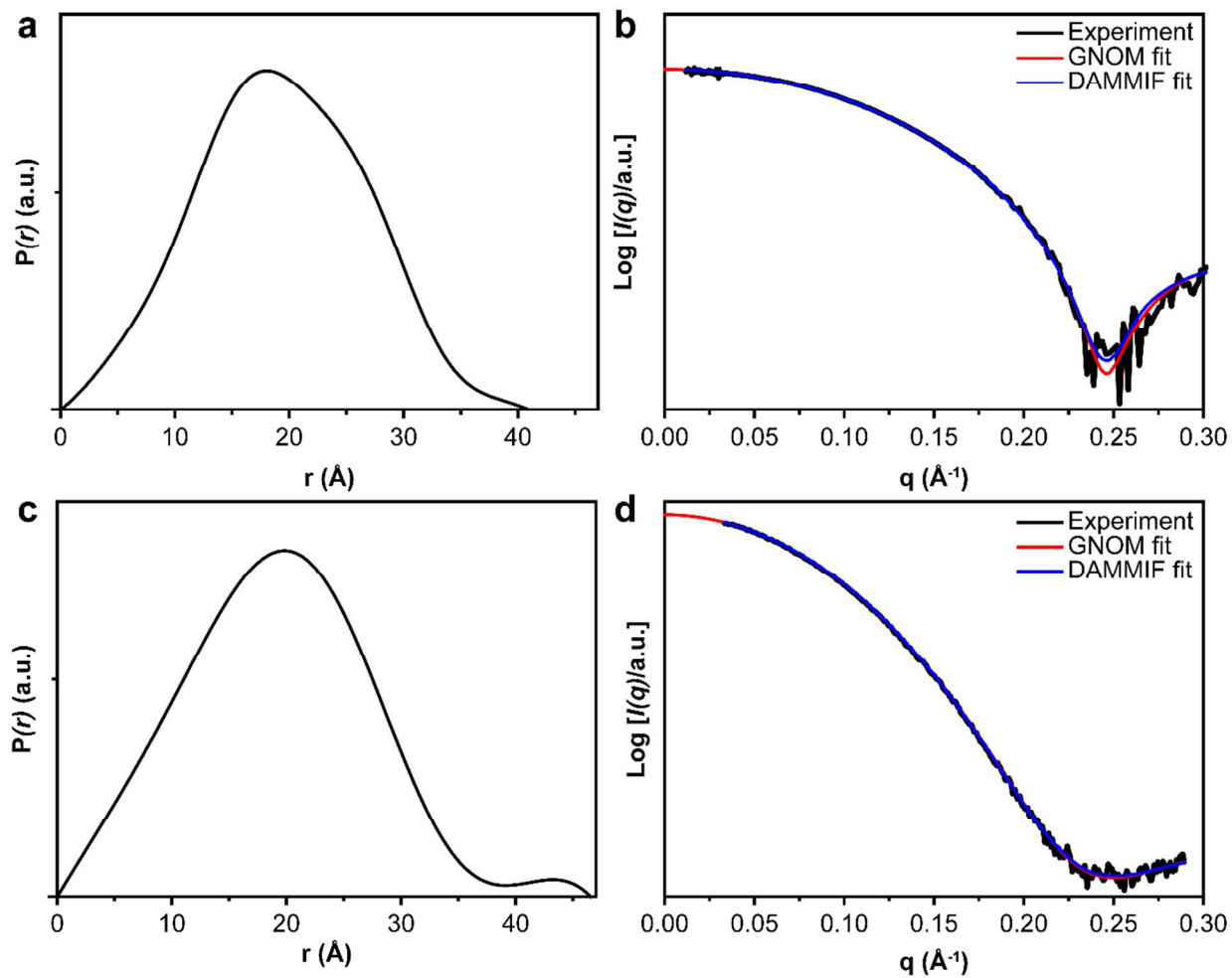


Figure S6. Pair distribution function (a, c) and comparison with GNOM-fit and DAMMIF-fit curves (b, d) from static SAXS data for PYP (a, b) and bleached PYP (c, d) for low-resolution shape reconstruction.

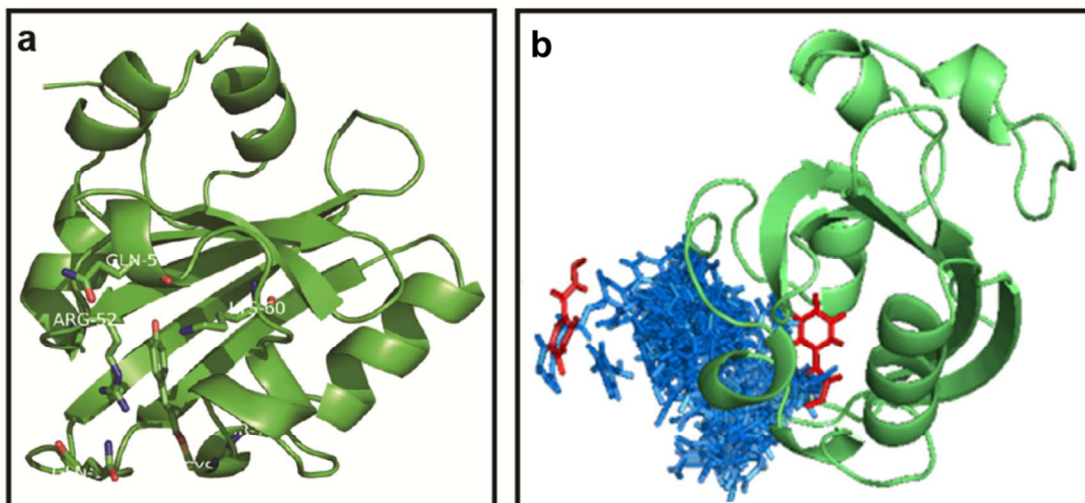


Figure S7. Chromophore migration after photo-detachment. (a) Amino acid residues interact with the chromophore via hydrogen bonds during migration in PYP and (b) chromophore migration from the interior active site to the exterior solvent. The image shows the exit of the chromophore from the protein. The starting position of the chromophore and the position of the chromophore after 100-ps simulation are shown in red stick representations; all other intermediate chromophore positions are shown in blue stick representations.

Table S1. Hydrogen bond and hydrophobic interactions between the chromophore and PYP body

Atoms in Chromophore	Atoms in PYP	Distance (Å)	Type
O1	*69:CYS:N	2.8	Hydrogen bond
O4'	42:TYR:OH	2.6	Hydrogen bond
O4'	46:GLU:OE2	2.5	Hydrogen bond
C6'	96:PHE:CG	3.6	Hydrophobic
C6'	96:PHE:CD1	3.8	Hydrophobic
C6'	96:PHE:CD2	3.4	Hydrophobic
C6'	96:PHE:CE2	3.5	Hydrophobic
C6'	96:PHE:CZ	3.8	Hydrophobic
C5'	50:THR:CG2	3.7	Hydrophobic
C5'	62:PHE:CE1	3.9	Hydrophobic
C5'	96:PHE:CD2	3.7	Hydrophobic
C5'	96:PHE:CE2	3.4	Hydrophobic
C5'	96:PHE:CZ	3.9	Hydrophobic
C4'	50:THR:CG2	3.4	Hydrophobic
C4'	62:PHE:CE1	3.9	Hydrophobic
C3'	66:VAL:CG1	3.8	Hydrophobic
C2'	52:ARG:CZ	3.6	Hydrophobic
C2'	66:VAL:CG1	3.9	Hydrophobic
C1'	67:ALA:CB	3.6	Hydrophobic
C1	69:CYS:CA	3.5	Hydrophobic
C1	69:CYS:CB	2.8	Hydrophobic
C1	98:TYR:CB	3.8	Hydrophobic
C2	67:ALA:CB	3.6	Hydrophobic
C2	96:PHE:CD1	3.8	Hydrophobic

* 69 amino acids. Abbreviated amino acid name: atom name and number.

Table S2. Number of hydrogen bonds between the chromophore and amino acid residues during migration

Amino acid residue	No. of chromophore interactions during migration
Cys69	10
Thr70	1
Arg52	22
Gln56	4
Lys60	3
Gln99	14

Table S3. Calculated potential energy of holo-PYP, PYP without the chromophore, and pB₂

	Potential energy (KJ/mol)	Pdb code
pG (crystal structure)	-6.6856934e+03	1NWZ
pG without chromophore	-6.4501738e+03	1NWZ (without chromophore)
pB ₂ (solution structure)	-4.8805411e+02	2KX6

* Force Field is Amber03

Reference

1. Imamoto, Y.; Ito, T.; Kataoka, M.; Tokunaga, F., Reconstitution photoactive yellow protein from apoprotein and p-coumaric acid derivatives. *FEBS Lett.* **1995**, *374* (2), 157-160.
2. Meyer, T. E.; Yakali, E.; Cusanovich, M. A.; Tollin, G., Properties of a water-soluble, yellow protein isolated from a halophilic phototrophic bacterium that has photochemical activity analogous to sensory rhodopsin. *Biochemistry* **1987**, *26* (2), 418-423.
3. Ahn, S.; Kim, K. H.; Kim, Y.; Kim, J.; Ihee, H., Protein tertiary structural changes visualized by time-resolved X-ray solution scattering. *The journal of physical chemistry. B* **2009**, *113* (40), 13131-13133.
4. Goldstein, H., *Classical Mechanics*. Addison-Wesley Publishing Company, Inc.: U.S.,1980.
5. Phillips, J. C.; Braun, R.; Wang, W.; Gumbart, J.; Tajkhorshid, E.; Villa, E.; Chipot, C.; Skeel, R. D.; Kalé, L.; Schulten, K., Scalable Molecular Dynamics with NAMD. *Journal of computational chemistry* **2005**, *26* (16), 1781-1802.
6. MacKerell, A. D.; Bashford, D.; Bellott, M.; Dunbrack, R. L.; Evanseck, J. D.; Field, M. J.; Fischer, S.; Gao, J.; Guo, H.; Ha, S.; Joseph-McCarthy, D.; Kuchnir, L.; Kuczera, K.; Lau, F. T. K.; Mattos, C.; Michnick, S.; Ngo, T.; Nguyen, D. T.; Prodhom, B.; Reiher, W. E.; Roux, B.; Schlenkrich, M.; Smith, J. C.; Stote, R.; Straub, J.; Watanabe, M.; Wiórkiewicz-Kuczera, J.; Yin, D.; Karplus, M., All-Atom Empirical Potential for Molecular Modeling and Dynamics Studies of Proteins. *The Journal of Physical Chemistry B* **1998**, *102* (18), 3586-3616.
7. Berman, H. M.; Westbrook, J.; Feng, Z.; Gilliland, G.; Bhat, T. N.; Weissig, H.; Shindyalov, I. N.; Bourne, P. E., The Protein Data Bank. *Nucleic Acids Research* **2000**, *28* (1), 235-242.